Electronic Supplementary Material (ESI) for Environmental Science: Nano.
This journal is © The Royal Society of Chemistry 2023

Support Information

Rational Design of Active Sites in Alumina-Based Catalysts to Optimize Antibonding-Orbital Occupancy for Tetrafluoromethane Decomposition

Tao Luo[a], Yingkang Chen[a], Kang Liu[a], Junwei Fu[a], Hang Zhang[a], Shanyong Chen[b], Qiyou Wang[a], Kejun Chen[a], Jun Wang[a], Wanru Liao[a], Hongmei Li[a], Zhang Lin[c], Min Liu[a,*]

[a] Hunan Joint International Research Center for Carbon Dioxide Resource Utilization, School of Physics and Electronics, Central South University, Changsha 410083, Hunan, P. R. China

[b] School of Chemistry and Chemical Engineering, Central South University, Changsha 410083, Hunan, P. R. China

[c] School of Metallurgy and Environment, Central South University, Changsha 410083, Hunan, P. R. China

*Corresponding author. E-mail address: minliu@csu.edu.cn (Min Liu)

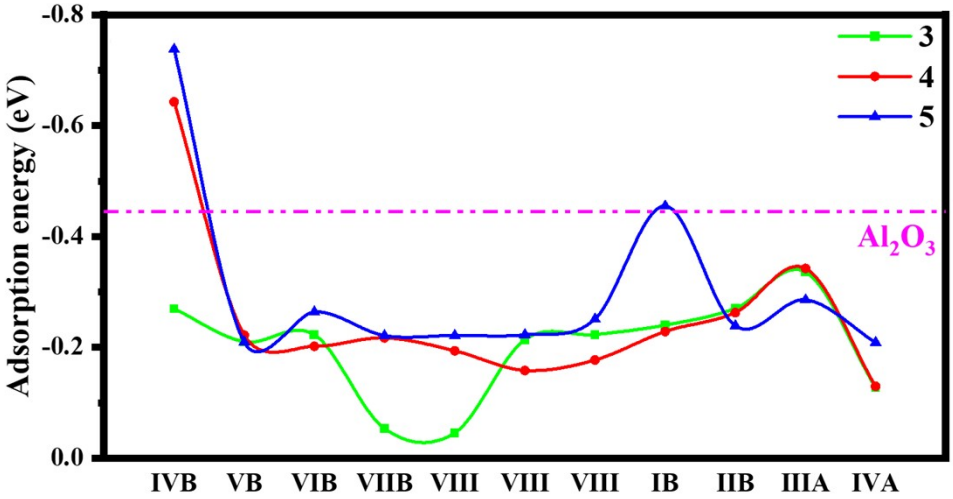

Figure. S1 The adsorption energy of CF_4 doped with different elements at the $1Al_{3C}$ site. The red dotted line is the CF_4 adsorption energy of the pure Al_2O_3 at the $1Al_{3C}$ site.

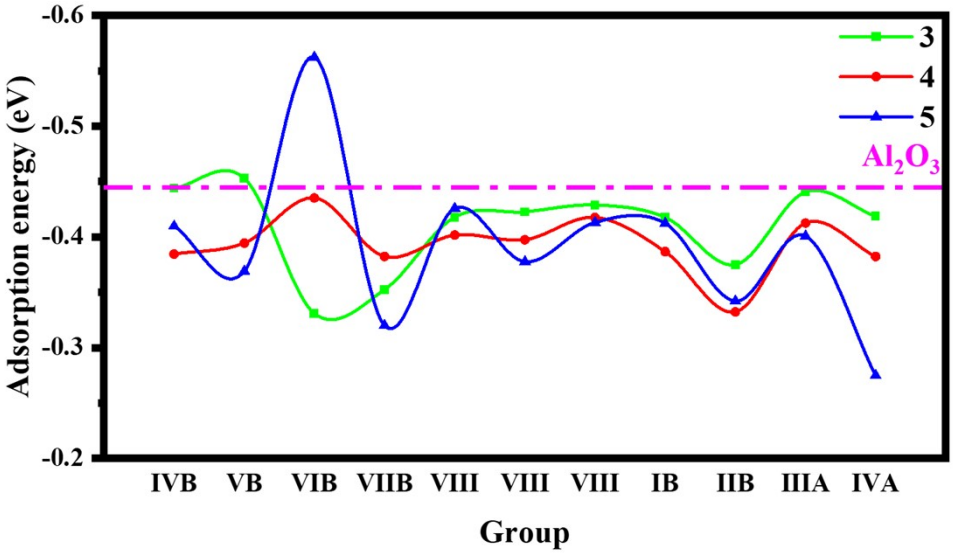

Figure. S2 The adsorption energy of CF_4 doped with different elements at the $2Al_{4C}$ site but with the active center at $1Al_{3C}$. The red dotted line is the CF_4 adsorption energy of the pure Al_2O_3 at the $1Al_{3C}$ site.

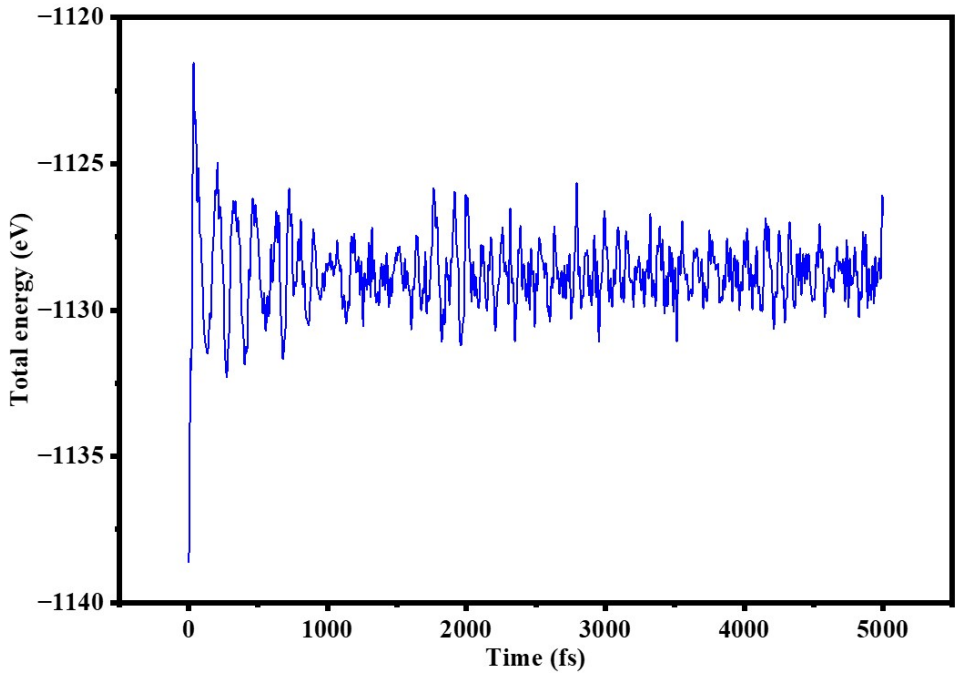

Figure. S3 Molecular dynamics stability of pure Al_2O_3 at 650 ℃ calculated by AIMD simulation.

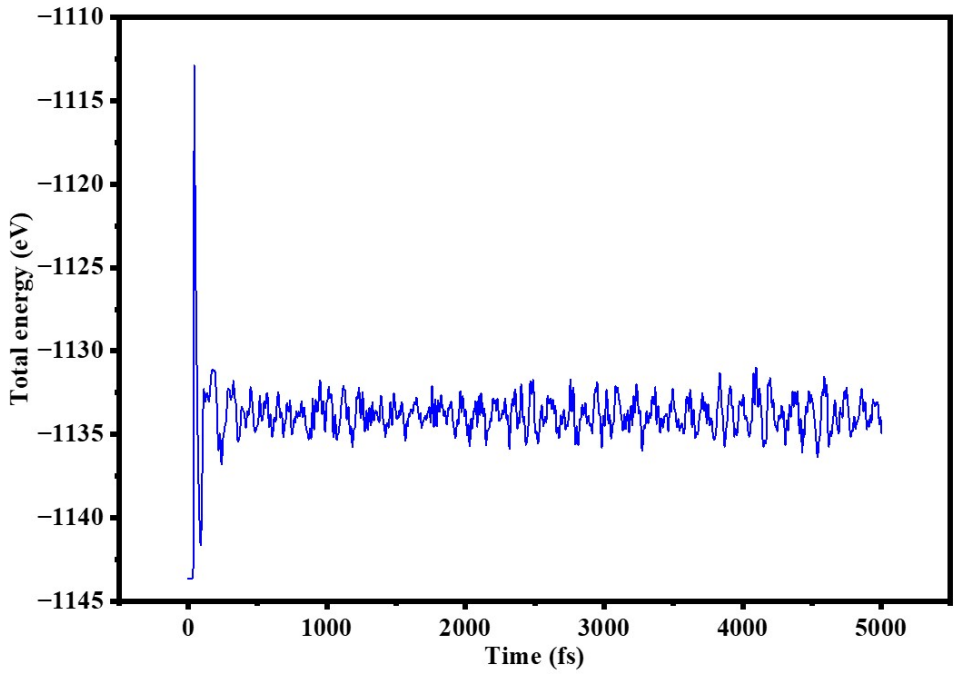

Figure. S4 Molecular dynamics stability of Zr-Al_2O_3 at 650C calculated by AIMD simulation for the best active site ($3Al_{4C}$).

Figure. S5 Molecular dynamics stability of Hf-Al_2O_3 at 650C calculated by AIMD simulation for the best active site ($3Al_{4C}$).

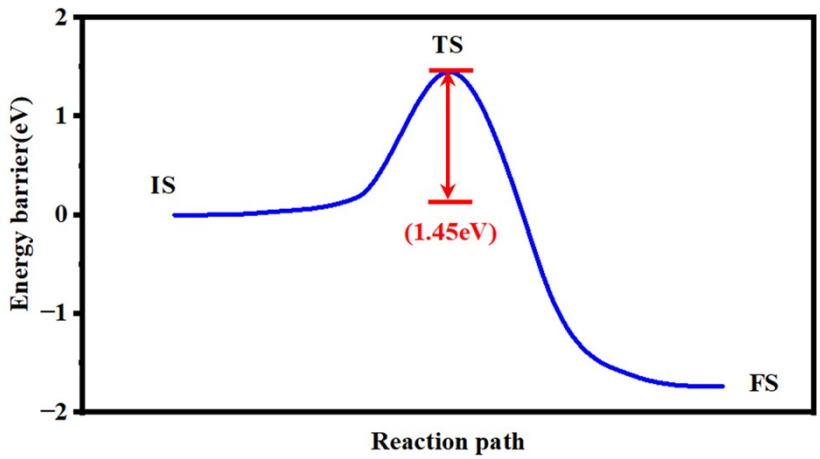

Figure S6. The activation energy barrier for the decomposition of CF_4 to F+CF_3 at the $1Al_{3C}$ site on the pure Al_2O_3 surface.

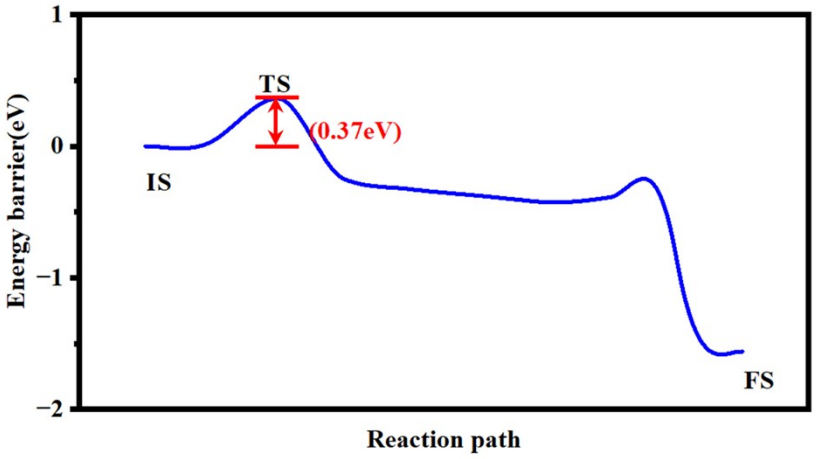

Figure S7. The activation energy barrier for the decomposition of CF_4 to F+CF_3 at the Zr site ($3Al_{4C}$) on the Zr-Al_2O_3 surface.

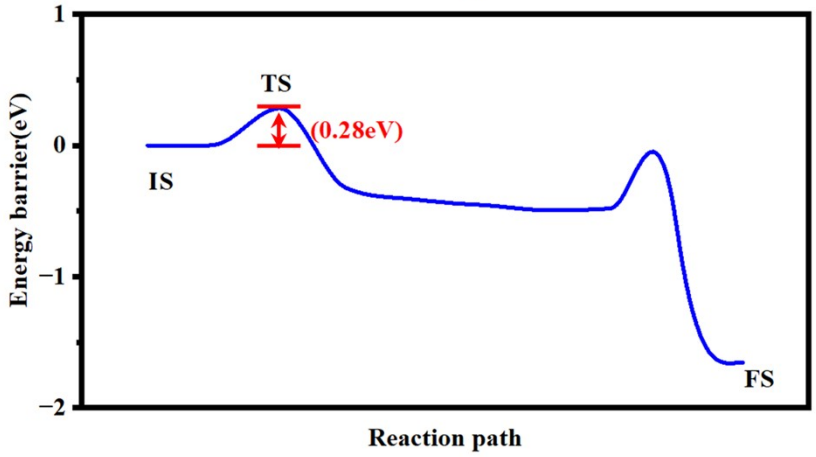

Figure S8. The activation energy barrier for the decomposition of CF_4 to F+CF_3 at the Hf site ($3Al_{4C}$) on the Hf-Al_2O_3 surface.

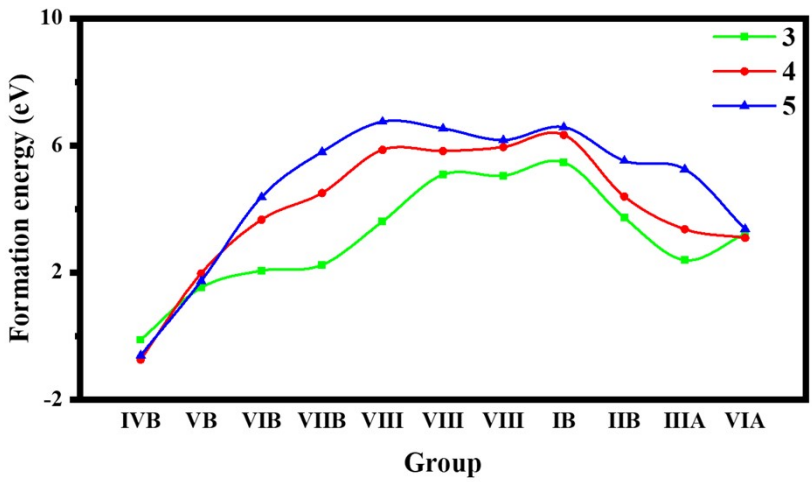

Figure. S9 The formation energy of different metal dopings at the $1Al_{3c}$ site.

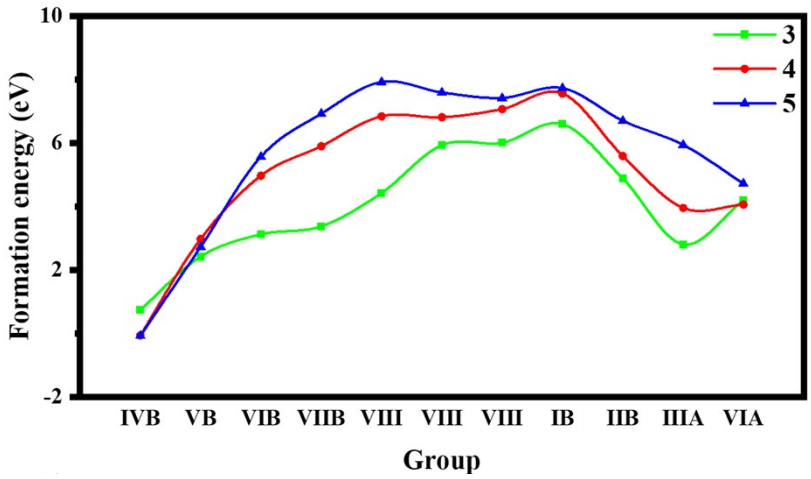

Figure. S10 The formation energy of different metal dopings at the $2Al_{4c}$ site.

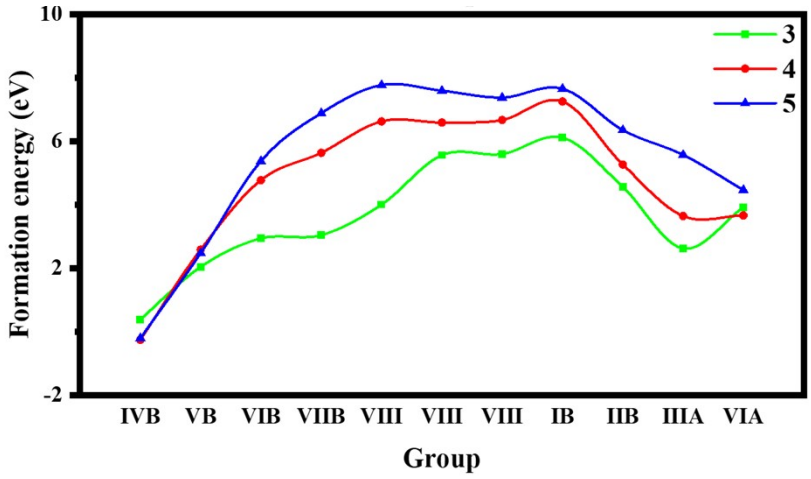

Figure. S11 The formation energy of different metal dopings at the $3Al_{4c}$ site.

Table. S1 Bader charge analysis of the C atom, different F atoms, and CF_4 molecule. F4 is the F atom closest to the adsorption site.

Site	C	F1	F2	F3	F4	CF_4
$Al(2Al_{4c})$	1.595	7.599	7.610	7.601	7.611	32.016
$Zr(2Al_{4c})$	1.634	7.575	7.583	7.581	7.609	31.981
$Hf(2Al_{4c})$	1.590	7.572	7.637	7.580	7.584	31.962
$Al(3Al_{4c})$	1.600	7.599	7.612	7.601	7.606	32.018
$Zr(3Al_{4c})$	1.621	7.565	7.614	7.588	7.592	31.981
$Hf(3Al_{4c})$	1.622	7.567	7.601	7.579	7.590	31.959

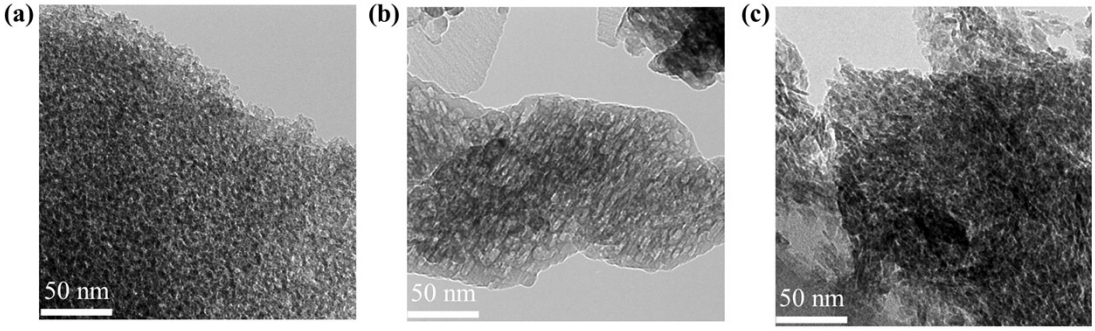

Figure. S12 TEM images of nanosheet morphology for Al_2O_3, Zr-Al_2O_3, Hf-Al_2O_3 catalysts

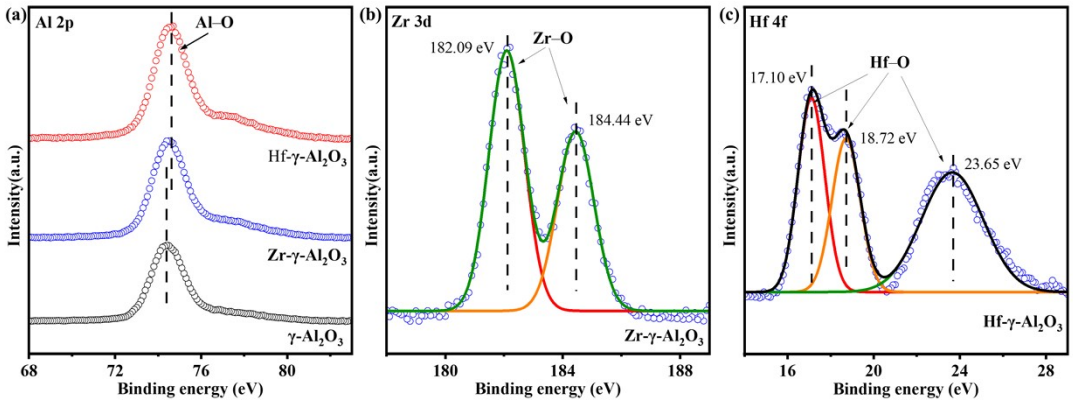

Figure. S13 X-ray photo electron spectroscopy (XPS) spectra of catalysts. (a) Al 2p of fresh. (b) Zr 3d of fresh. (c) Hf 4f of fresh.

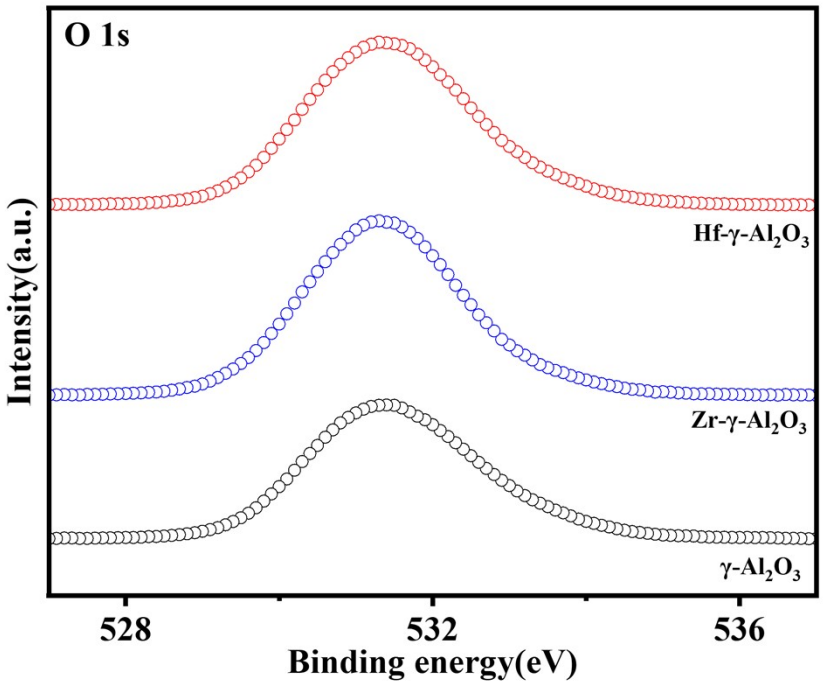

Figure. S14 XPS spectra of O 1s for Al_2O_3, Zr-Al_2O_3, Hf-Al_2O_3 catalysts.

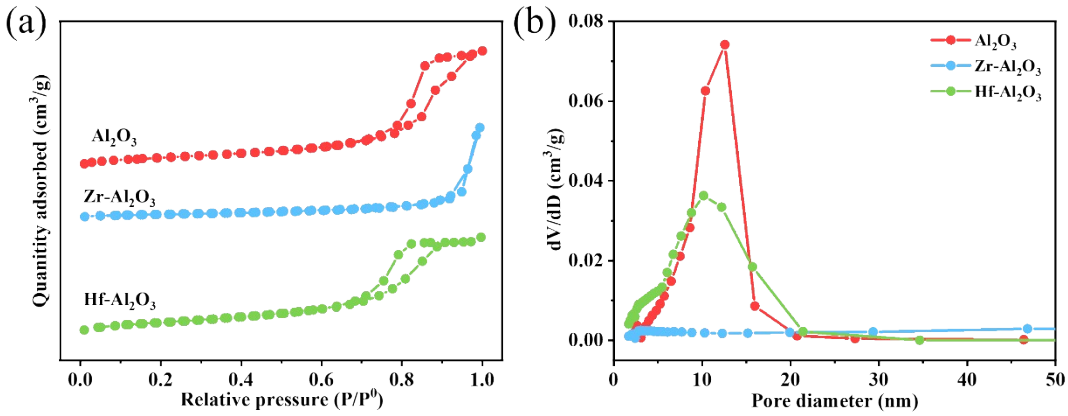

Fig. S15 (a) N_2 adsorption-desorption curve and (b) pore diameter distribution of Al_2O_3, Zr-Al_2O_3 and Hf-Al_2O_3 catalysts.

Table 2. BET results of Al_2O_3, Zr-Al_2O_3 and Hf-A_2O_3 catalysts.

Sample	SA (m^2 g^{-1})	PV (cm^3 g^{-1})	APR (nm)
Al_2O_3	136.7	0.49	11.9
Zr-Al_2O_3	53.12	0.38	5.69
Hf-Al_2O_3	86.96	0.42	9.76